REPORT DOCUMENTATION PAGE

Form Approved OMB NO. 0704-0188

1. REPORT DATE (DD-MM-YYYY)	2. REPORT TYPE	3. DATES COVERED (From - To)
	New Reprint	-

4. TITLE AND SUBTITLE
Crystal structure prediction for cyclotrimethylene trinitramine (RDX) from ?rst principles

5a. CONTRACT NUMBER
W911NF-09-1-0397

5b. GRANT NUMBER

5c. PROGRAM ELEMENT NUMBER
611102

6. AUTHORS
Rafal Podeszwa, Betsy M. Rice, and Krzysztof Szalewicz

5d. PROJECT NUMBER

5e. TASK NUMBER

5f. WORK UNIT NUMBER

7. PERFORMING ORGANIZATION NAMES AND ADDRESSES
University of Delaware
Vice Provost for Research
University of Delaware
Newark, DE 19716 -

8. PERFORMING ORGANIZATION REPORT NUMBER

9. SPONSORING/MONITORING AGENCY NAME(S) AND ADDRESS(ES)
U.S. Army Research Office
P.O. Box 12211
Research Triangle Park, NC 27709-2211

10. SPONSOR/MONITOR'S ACRONYM(S)
ARO

11. SPONSOR/MONITOR'S REPORT NUMBER(S)
53252-CH.2

12. DISTRIBUTION AVAILIBILITY STATEMENT
Approved for public release; federal purpose rights

13. SUPPLEMENTARY NOTES
The views, opinions and/or findings contained in this report are those of the author(s) and should not contrued as an official Department of the Army position, policy or decision, unless so designated by other documentation.

14. ABSTRACT
Crystal structure prediction and molecular dynamics methods were applied to the cyclotrimethylene trinitramine (RDX) crystal to explore the stability rankings of various polymorphs using a recently developed nonempirical potential energy function that describes the RDX dimer interactions. The energies of 500 high-density structures resulting from molecular packing were minimized and the 14 lowest-energy structures were subjected to isothermal–isostress molecular dynamics (NsT-MD) simulations. For both crystal

15. SUBJECT TERMS
symmetry-adapted perturbation theory, crystal structure

16. SECURITY CLASSIFICATION OF:			17. LIMITATION OF ABSTRACT	15. NUMBER OF PAGES	19a. NAME OF RESPONSIBLE PERSON
a. REPORT	b. ABSTRACT	c. THIS PAGE			Krzysztof Szalewicz
UU	UU	UU	UU		19b. TELEPHONE NUMBER: 302-831-6579

Report Title

Crystal structure prediction for cyclotrimethylene trinitramine (RDX) from ?rst principles

ABSTRACT

Crystal structure prediction and molecular dynamics methods were applied to the cyclotrimethylene trinitramine (RDX) crystal to explore the stability rankings of various polymorphs using a recently developed nonempirical potential energy function that describes the RDX dimer interactions. The energies of 500 high-density structures resulting from molecular packing were minimized and the 14 lowest-energy structures were subjected to isothermal–isostress molecular dynamics (NsT-MD) simulations. For both crystal structure prediction methods and molecular dynamics simulations, the lowest-energy polymorph corresponded to the experimental structure; furthermore, the lattice energy of this polymorph was lower than that of the other polymorphs by at least 1.1 kcal/mol.

Crystal parameters and densities of the low-energy crystal produced by the NsT-MD simulations matched those of the experimental crystal to within 1% of density and cell edge lengths and 0.011 of the cell angle. The arrangement of the molecules within the time-averaged unit cell were in equally outstanding agreement with experiment, with the largest deviation of the location of the molecular mass centers being less than 0.07 A and the largest deviation in molecular orientation being less than 2.81. NsT-MD simulations were also used to calculate crystallographic parameters as functions of temperature and pressure and the results were in a reasonable agreement with experiment.

REPORT DOCUMENTATION PAGE (SF298)
(Continuation Sheet)

Continuation for Block 13

ARO Report Number 53252.2-CH
Crystal structure prediction for cyclotrimethylene ...

Block 13: Supplementary Note

Approved for public release; federal purpose rights

Crystal structure prediction for cyclotrimethylene trinitramine (RDX) from first principles†

Rafal Podeszwa,*[ab] Betsy M. Rice[c] and Krzysztof Szalewicz[b]

Received 4th February 2009, Accepted 25th March 2009
First published as an Advance Article on the web 28th April 2009
DOI: 10.1039/b902015b

Crystal structure prediction and molecular dynamics methods were applied to the cyclotrimethylene trinitramine (RDX) crystal to explore the stability rankings of various polymorphs using a recently developed nonempirical potential energy function that describes the RDX dimer interactions. The energies of 500 high-density structures resulting from molecular packing were minimized and the 14 lowest-energy structures were subjected to isothermal–isostress molecular dynamics (NsT-MD) simulations. For both crystal structure prediction methods and molecular dynamics simulations, the lowest-energy polymorph corresponded to the experimental structure; furthermore, the lattice energy of this polymorph was lower than that of the other polymorphs by at least 1.1 kcal mol^{-1}. Crystal parameters and densities of the low-energy crystal produced by the NsT-MD simulations matched those of the experimental crystal to within 1% of density and cell edge lengths and 0.01° of the cell angle. The arrangement of the molecules within the time-averaged unit cell were in equally outstanding agreement with experiment, with the largest deviation of the location of the molecular mass centers being less than 0.07 Å and the largest deviation in molecular orientation being less than 2.8°. NsT-MD simulations were also used to calculate crystallographic parameters as functions of temperature and pressure and the results were in a reasonable agreement with experiment.

1. Introduction

Prediction of a crystal structure using only information about the atomic arrangement of a constituent molecule was once considered impossible.[1–4] While the structure of various conformations of individual molecules can be readily determined on current computational architectures using highly-correlated quantum mechanical methods, there are substantial challenges that preclude the prediction of the crystalline state structures of even fairly small organic molecules. The issue lies with properly representing the binding forces within molecular crystals: van der Waals interactions. Such forces can be modelled *ab initio* by well-established methods of quantum chemistry. However, the high computational cost of such approaches has prevented extensive applications of these methods to molecular crystals. The only computationally feasible quantum mechanics-based approach for treating molecular crystals is density functional theory (DFT). Unfortunately, DFT has been shown to be inaccurate for systems in which the dispersion components of van der Waals forces are dominant (see, *e.g.*, ref. 5). This problem extends to DFT calculations for molecular crystals with periodic boundary conditions.[6,7] Empirical models using simple atom–atom potentials can be used to predict crystal structures, but rely on limited experimental information (possibly supplemented by some quantum mechanical calculations) for parameterization. Consequently, atomistic simulations using such models often produce unsatisfactory results in describing systems or conditions outside of those included in the fitting data. All of these factors have made the prediction of crystal structure using information from only the molecular structure rather unsuccessful.[1–4,8]

Recently, we demonstrated[9,10] that potential energy functions fitted to calculations using a novel method, symmetry-adapted perturbation theory based on the density-functional description of the monomers [SAPT(DFT)],[11–13] provide sufficient accuracy and numerical efficiency for predicting the crystal structure properties of the molecular crystal of cyclotrimethylene trinitramine (RDX). Also, for the benzene crystal at the experimental geometry, the SAPT(DFT) interaction energies,[14] together with three-body SAPT(DFT) non-additive corrections,[15] yielded the lattice energy accurate to within a few percent of the experimental values,[9] significantly better than other methods based on first principles.[16,17] The work of ref. 9 and 10 was based on a six-dimensional potential fitted to over 1100 single-point calculations for the RDX dimer using the SAPT(DFT) method. We first used this potential in isothermal–isostress molecular dynamics (NsT-MD) simulations of crystalline RDX at ambient conditions for the experimentally observed structure.[10] We showed that the crystallographic parameters and molecular configurations were in excellent agreement with measured values. In the

[a] *Institute of Chemistry, University of Silesia, Szkolna 9, 40-006, Katowice, Poland*
[b] *Department of Physics and Astronomy, University of Delaware, DE 19716, Newark*
[c] *U.S. Army Research Laboratory, Aberdeen Proving Ground, MD 21005*

† Electronic supplementary information (ESI) available: Maximum absolute deviations of molecular parameters from corresponding values in an ideal RDX crystal; experimental and predicted orientational parameters of symmetry equivalent molecules in RDX unit cell. See DOI: 10.1039/b902015b

current study, which extends and supplements the work described in ref. 9, we use the SAPT(DFT) potential of the RDX dimer in NsT-MD simulations of several hypothetical RDX crystal structures, where the initial configurations are obtained using crystal structure prediction methods. This work will explore several structural phases of RDX other than those observed experimentally, and the role of thermal effects on the stability rankings. Additionally, the temperature and pressure dependencies of crystallographic parameters for the experimentally observed polymorph will be determined from NsT-MD simulations.

Simultaneously with our work,[9,10] the goal of predicting crystal structures was achieved by two other groups. The method of Misquitta *et al.*,[18] successfully applied in a prediction of the lowest-energy structure of the crystal of $C_6Br_2ClFH_2$, also uses SAPT(DFT) and can be viewed as a simplification of the approach used by us. The main differences are in the treatment of the induction and dispersion energies and of their exchange counterparts. Whereas we compute all these terms for the whole set of dimer configurations, Misquitta *et al.* approximate them by a damped asymptotic expansion. There are also differences in the generation and ranking of polymorphs. In both cases, a large number of polymorph candidates is first generated, then a subset of polymorphs is subjected to lattice energy minimizations (a 0 K simulation). In our study, the minimizations are followed by NsT-MD simulations at ambient conditions, thus introducing thermal effects. We will further elaborate on these calculations below.

A very different approach was developed by Neumann *et al.*[19] These authors first fitted a simple atom–atom potential function for a given system to lattice energies computed using the DFT + D (DFT plus asymptotic dispersion) method of Neumann and Perrin[20] and applied it in lattice energy minimization. For a number of lowest-energy polymorphs predicted by this potential, they perform further optimizations with "on-the-fly" DFT + D calculations. This approach works reasonably well, despite the known problems of the standard DFT method in computing interaction energies which cannot be solved just by a simple addition of true dispersion energies.[5] To overcome this problem, Neumann and Perrin[20] introduced a "damping" function in the dispersion component with parameters optimized to reproduce experimental lattice parameters for about 30 crystals of small molecules. Thus, this DFT + D method includes a significant degree of empiricism, in contrast to our SAPT(DFT)-based approach which is completely nonempirical.

Computational details

Crystal structure predictions for RDX

Our first goal is to generate probable RDX crystal structures using information only about the molecular structure. Several approaches have been developed to generate and rank probable crystal structures.[21] We used a method developed specifically for molecular energetic materials[22,23] which should be appropriate for the system under study here. In the first step of this procedure, a three-dimensional molecular model of the constituent molecule (monomer) is generated. Here, we used the rigid monomer's structure corresponding to that measured in the crystal at ambient conditions.[24] Next, crystals of different symmetries are created using this monomer's structure and the MOLPAK (molecular packing) software suite.[22] MOLPAK produces crystals corresponding to molecular coordination geometries observed in the most common space groups of molecular crystals; descriptions of coordination geometries are given in ref. 22 and 25. The version of MOLPAK used in this study[25] samples 51 coordination geometries corresponding to the triclinic ($P1$, $P\bar{1}$), monoclinic ($P2_1$, $P2_1/c$, Cc, $C2$, $C2/c$, Pc, $P2/c$, $P2_1/m$, $P2/m$, $P2$, Pm, $P2/m$), and orthorhombic (Z = 4, $P2_12_12$, $P2_12_12_1$, $Pca2_1$, $Pna2_1$, $Pnn2$, $Pba2$, $Pnc2$, $P222_1$, $Pmn2_1$, $Pma2$, Z = 8, $Pbcn$, $Pbca$) space groups. These coordination geometries were found *via* a crystal database search as described in ref. 22 and Appendix 1 of ref. 25. For each hypothetical crystal generated, an initial arrangement of the atoms within the unit cell is obtained by first orienting the monomer in a Cartesian coordinate system whose origin is located at the centroid of the monomer. The remaining symmetry-equivalent entities are then generated using the appropriate space group symmetry operations and coordinate geometry definition as described in ref. 22. Sampling of possible orientations of the molecules within each coordination geometry is performed by a systematic angular sweep of the range $\pm$ 90° in 10° steps. This sampling results in the generation of 6,859 (19^3) hypothetical crystal structures per coordination geometry. The intermonomer separations were then varied for each hypothetical structure until a minimum-volume packing based on a repulsion criterion is reached as described in ref. 22 and Appendix 1 of ref. 25. In this way, the MOLPAK step generated 6,859 $\times$ 51 hypothetical crystals which could be rank-ordered by density. Next, rigid-molecule lattice energy minimizations were performed on the 500 highest-density candidates using the WMIN lattice energy optimization codes.[26] In this procedure, the cell parameters, location, and orientations of the molecules are optimized within space group symmetry constraints using the potential function described hereafter. The starting values of these parameters were those generated by the MOLPAK step. The coordination geometries are not, in general, preserved by WMIN during the energy minimization and the geometries given in the tables denote only the starting configurations. In order to identify duplicate crystal structures produced during the WMIN lattice energy minimization step, reduced cell parameters are compared, since such parameters provide a unique representation of a crystal lattice.

The WMIN lattice energy program cannot, at this time, accommodate the more complicated published form of the SAPT(DFT) potential.[10] Rather, WMIN requires that the lattice energy be described by a sum of intermolecular atom–atom terms including the exponential, inverse sixth power, and Coulomb functions:

$$V_{\alpha\beta}(r) = A_{\alpha\beta}\exp(-B_{\alpha\beta}r) - C_{\alpha\beta}/r^6 + V^C_{\alpha\beta}(r), \qquad (1)$$

where

$$V^C_{\alpha\beta}(r) = \frac{q_\alpha q_\beta}{r}. \qquad (2)$$

Table 1 Parameters for SAPT(DFT)$_{exp-6}$ potential used in the MOLPAK/WMIN calculations

Pair (α–β)	$A_{\alpha\beta}$/kcal mol^{-1}	$B_{\alpha\beta}$/Å^{-1}	$C_{\alpha\beta}$/Å^6 kcal mol^{-1}
C–C	2400957.6219	4.7141	331.7437
N–C	−380.0979	2.0758	266.5829
N–N	899731.7524	4.7263	214.2209
O–C	359683.8587	4.3728	322.4757
O–N	112623.7784	4.2737	259.1353
O–O	42389.9472	3.7509	313.4666
H–C	431554.8893	6.0138	172.4754
H–N	926.9395	2.5410	138.5979
H–O	6939.8408	3.6332	167.6569
H–H	2647.1147	3.4678	89.6709

In these formulas, r is the interatomic distance between atoms α and β, q_α and q_β are the permanent electric charges on the atoms, and the remaining quantities are adjustable parameters of the fit (we will denote this potential as "exp-6"). Therefore, we fitted an exp-6 form (denoted hereafter as SAPT(DFT)$_{exp-6}$) to the SAPT(DFT) points used to generate the SAPT(DFT) potential and used this function in crystal structure prediction methods. The parameters of SAPT(DFT)$_{exp-6}$ are given in Table 1. The charges are the same as in ref. 10. The coefficients $C_{\alpha\beta}$ were fitted assuming the combining rule: $C_{\alpha\beta} = \sqrt{C_{\alpha\alpha}C_{\beta\beta}}$ and, therefore, only the diagonal elements in the last column of Table 1 are independent.

NsT-MD simulations of polymorphs of RDX

NsT-MD simulations using the DL_POLY version 2 suite of molecular dynamics simulation software[27] and the SAPT(DFT) potential of the RDX dimer[10] were performed for the 14 lowest-energy crystal structures generated by the MOLPAK/WMIN calculations described above. The rigid-molecule approximation was assumed and symmetry constraints were not imposed. The supercells used in these simulations were composed of blocks of unit cells, with the contents initially arranged in the configuration corresponding to that of the structure produced by the WMIN/SAPT(DFT)$_{exp-6}$ optimization. The sizes were selected to ensure that the perpendicular widths between opposing faces of the simulation cell were at least twice the interaction potential cutoff distance (12.0 Å). Coulombic interactions were handled using Ewald summations. Atomic velocities corresponding to T = 298 K were then assigned and a trajectory of 30 000 steps (1 time step = 1 fs) was performed to equilibrate the system. The atomic velocities were scaled at every 5th step during this equilibration trajectory to drive the system to the desired temperature more rapidly.

A subsequent NsT-MD trajectory consisting of 100 000 steps was then performed in which thermodynamic properties and crystal parameters were averaged; atomic configurations were also recorded at every 500th step during the production trajectory. The snapshots were used to generate time-averaged information about the locations and orientations of the molecules within the unit cells. These are given in terms of center-of-mass fractional coordinates (s_x, s_y, s_z) and the Euler angles (θ, ϕ, ψ) that transform the principal axes of inertia of each molecule to its space-fixed coordinate system (*i.e.*, the Cartesian axes). For each polymorphic form studied, the molecular parameters for each of the symmetry-equivalent molecules in the unit cell were averaged over time and over all unit cells within the simulation supercell.

Results

Table 2 provides the MOLPAK/WMIN/SAPT(DFT)$_{exp-6}$ predictions of the density and lattice energy (per molecule) for the lowest-energy crystal for each of the 51 coordination geometries sampled in this study (*i.e.*, only the global minimum for all packing/minimizatons starting from a given coordination geometry is given). Many of the MOLPAK structures that belong to the same space group but have different coordination geometries used in the packing portion of the calculation (*e.g.*, CB and CC) converged to the same minimum in the WMIN lattice energy refinement step. Also, there are numerous instances in which crystals in different space groups/coordination geometries have similar lattice energies and densities; however, comparisons of reduced cell parameters for such cases indicate that these crystals are not duplicates. As evident in Table 2, the lowest-energy crystal (the same structure was obtained in optimizations starting from coordination geometries CB and CC) is lower in energy than

Table 2 Density and lattice energy of the lowest-energy crystal for each starting coordination geometry generated in the MOLPAK/WMIN/SAPT(DFT)$_{exp-6}$ calculations

Space group	Coordination geometry	ρ/g cc^{-1}	E/kcal mol^{-1}
Pbca	CB, CC	1.860	−31.67
$P2_1/c$	AM, FC	1.848	−29.73
$P2_1/c$	AI	1.814	−29.63
$P2_1/c$	AK	1.849	−29.28
$P2_12_12_1$	AQ, AZ	1.751	−28.54
$Pna2_1$	AV, BD, AU, AS	1.749	−28.52
$C2/c$	DD	1.748	−27.79
$Pca2_1$	AY	1.749	−27.73
$P2_1$	AH, AF	1.758	−27.71
$P2_1/c$	FA	1.843	−27.68
$Pca2_1$	BH	1.784	−27.63
$P\bar{1}$	AB, CA	1.785	−27.48
$C2/c$	DC, DE	1.765	−27.28
$P1$	AA	1.705	−27.17
Cc	DA	1.683	−27.17
Pbcn	CD	1.739	−27.15
$P2_12_12_1$	AP	1.712	−26.98
$Pna2_1$	BF	1.740	−26.77
Pbcn	CE	1.743	−26.61
$P2_12_12_1$	BA	1.709	−26.53
Pc	AD	1.683	−26.31
$P2_12_12_1$	BB	1.677	−26.26
Pc	AG	1.651	−26.23
*C*2	DB	1.727	−25.89
*P*2/*c*	AJ, AL, FD	1.711	−25.57
*Pnn*2	AR, AT	1.604	−25.36
*Pnn*2	BE	1.631	−25.35
*Pba*2	AW, BG	1.693	−25.29
*Pnc*2	BI	1.631	−24.49
*Pnc*2	AX	1.630	−24.48
$P2_1/m$	AN	1.646	−24.28
*P*2/*m*	FB	1.646	−24.28
*P*2	AE	1.665	−23.86
$P222_1$	BC	1.641	−23.68
$Pmn2_1$	BJ	1.508	−23.66
*Pma*2	BK	1.599	−22.54
Pm	AC	1.323	−18.68
*P*2/*m*	AO	1.395	−18.44

Table 3 Comparison of lattice energies and crystallographic parameters calculated using WMIN/SAPT(DFT)$_{exp\text{-}6}$[a] and NsT-MD/SAPT(DFT)[b] methods

Space group	Coord. group	Soln No.	E/kcal mol^{-1}	Density[c]/g cc^{-1}		a/Å[c]		b/Å[c]		c/Å[c]		α/°[d]		β/°[d]		γ/°[d]		$\Delta\theta$/°[e]	Δx[e]/Å
Experiment (ref. 24)																			
Pbca				1.806		13.182		11.574		10.709		90.00		90.00		90.00			
Predictions[ab]																			
Pbca	CB	1	−31.67	1.860		13.094		11.483		10.546		90.00		90.00		90.00			
			−30.90	1.792	(−3.7)	13.234	(1.1)	11.609	(1.1)	10.720	(1.6)	90.00	(0.00)	89.99	(−0.01)	90.00	(0.00)	3.0	0.18
Pbca	CB	2	−30.62	1.829		13.217		11.505		10.605		90.00		90.00		90.00			
			−29.78	1.756	(−4.0)	13.377	(1.2)	11.682	(1.5)	10.755	(1.4)	90.00	(0.00)	89.99	(−0.01)	90.01	(0.01)	2.4	0.14
$P2_1/c$	AM	1	−29.73	1.848		8.145		10.505		9.396		90.00		96.80		90.00			
			−28.38	1.766	(−4.5)	8.132	(−0.2)	10.702	(1.9)	9.662	(2.8)	90.01	(0.01)	96.41	(−0.39)	89.99	(−0.01)	8.7	0.23
$P2_1/c$	AM	2	−29.63	1.814		7.127		11.386		10.532		90.00		72.13		90.00			
			−28.35	1.717	(−5.3)	7.236	(1.5)	11.683	(2.6)	10.719	(1.8)	90.00	(0.00)	71.46	(−0.67)	90.00	(0.00)	2.6	0.30
$P2_1/c$	AM	3	−29.59	1.815		7.691		10.585		9.998		90.00		87.14		90.00			
			−28.01	1.710	(−5.8)	7.887	(2.5)	10.854	(2.5)	10.092	(0.9)	90.00	(0.00)	87.39	(0.24)	90.00	(0.00)	1.5	0.22
$P2_1/c$	AM	4	−29.56	1.840		6.327		9.663		13.119		90.00		91.77		90.00			
			−27.48	1.731	(−6.0)	6.517	(3.0)	9.807	(1.5)	13.344	(1.7)	89.99	(−0.01)	91.31	(−0.46)	89.97	(−0.03)	4.4	0.25
$P2_1/c$	AI	1	−29.44	1.840		9.338		10.489		13.295		90.00		141.99		90.00			
			−28.24	1.770	(−3.8)	9.573	(2.5)	10.662	(1.7)	13.403	(0.8)	90.00	(0.00)	142.47	(0.48)	90.00	(0.00)	1.4	0.16
$P2_1/c$	AK	1	−29.28	1.849		9.850		10.086		11.735		90.00		136.82		90.00			
			−26.27	1.700	(−8.0)	10.402	(5.6)	10.178	(0.9)	12.270	(4.6)	90.00	(0.00)	138.10	(1.28)	90.00	(0.00)	3.4	0.58
$P2_1/c$	AM	5	−29.24	1.803		7.030		11.420		10.803		90.00		109.33		90.00			
			−28.09	1.714	(−4.9)	7.092	(0.9)	11.712	(2.6)	11.034	(2.1)	90.00	(0.00)	110.14	(0.81)	89.99	(−0.01)	3.6	0.31
Pbca	CB	3	−28.85	1.780		10.278		13.058		12.353		90.00		90.00		90.00			
			−27.42	1.702	(−4.4)	10.630	(3.4)	13.219	(1.2)	12.338	(−0.1)	90.00	(0.00)	90.00	(0.00)	90.01	(0.01)	2.9	0.31
$P2_1/c$	AK	2	−28.75	1.783		9.808		11.186		12.410		90.00		142.58		90.00			
			—	—		—		—		—		—		—		—		—	—
Pbca	CB	4	−28.57	1.772		10.236		12.903		12.609		90.00		90.00		90.00			
			−27.43	1.702	(−3.9)	10.627	(3.8)	13.225	(2.5)	12.335	(−2.2)	90.00	(0.00)	90.01	(0.01)	90.00	(0.00)	16.30	0.36
$P2_12_12_1$	AQ	1	−28.54	1.751		10.015		12.897		6.521		90.00		90.00		90.00			
			−28.33	1.681	(−4.0)	10.214	(2.0)	13.184	(2.2)	6.517	(−0.1)	89.99	(−0.01)	90.00	(0.00)	90.01	(0.01)	4.8	0.24
$Pna2_1$	AV	1	−28.52	1.749		15.223		8.420		6.579		90.00		90.00		90.00			
			−24.95	1.609	(−8.0)	15.208	(−0.1)	9.079	(7.8)	6.640	(0.9)	90.00	(0.00)	89.99	(−0.01)	89.99	(−0.01)	4.3	0.53

[a] WMIN/SAPT(DFT)$_{exp\text{-}6}$ values are given in the first line in each entry and represent a 0 K result. [b] NsT-MD/SAPT(DFT) values are given in the second line in each entry, and are time averaged results at T = 298 K, 1 atm. [c] Percent difference of NsT-MD results (T = 298 K) from MOLPAK results (T = 0 K) given in parentheses. [d] Difference given in parentheses. [e] Factors $\Delta\theta$ and Δx are the maximum absolute rigid-body rotational displacement (in °) and translational displacement (in Å) of any of the symmetry equivalent molecules in the time-averaged unit cell relative to the MOLPAK/WMIN counterpart.

all other low-energy crystals for the remaining coordination geometries by at least 1.94 kcal mol^{-1}.

Table 3 provides crystallographic parameters (given in the conventional setting rather than reduced cell representations) for the 14 lowest-energy crystal structures generated from calculations using the MOLPAK/WMIN procedure and the $SAPT(DFT)_{exp\text{-}6}$ potential. Several structures appearing in Table 3 that were not present in Table 2 are subsequent local minima for packing/minimizatons starting from a given coordination geometry. In particular, the AM geometry of the $P2_1/c$ group contributes a large number of low-energy minima. The solutions are numbered with increasing energy separately for each coordination geometry (column 3). Also in Table 3, the time-averaged crystallographic parameters for 13 of the corresponding crystals produced from NsT-MD simulations using the SAPT(DFT) potential are provided for comparison. In one case, the crystal produced by the simulation did not resemble the starting structure (MOLPAK/WMIN solution 2, coordination geometry AK, space group $P2_1/c$), thus suggesting that this structure is not a stable minimum on the SAPT(DFT) potential energy surface. No further analysis regarding this issue was performed.

In order to determine whether space group symmetry was preserved during the NsT-MD simulations for each polymorph, a unit cell for a hypothetical ideal RDX crystal was generated by applying the appropriate crystalline space group operations to averaged atomic positions for one of the symmetry-equivalent molecules in the time-averaged unit cell produced from the NsT-MD simulation. The molecular parameters (center-of-mass fractionals and orientational Euler angles) of the time-averaged unit cells were then compared with those of the "ideal" crystals. Table S1 of the ESI† provides the maximum deviations of the monomer's positions and orientations in the time-averaged unit cells from those of the ideal RDX crystals. The maximum deviation of the center-of-mass fractional coordinates from ideality among all of the polymorphs is 0.0032 fractional units (solution 2, AM) and the maximum deviation of Euler angles from ideality is 3.01° (solution 1, AK). The good agreement of the NsT-MD averaged values with those of ideal crystals demonstrate that the crystalline space group symmetries are well maintained throughout the simulations for these polymorphs.

Deviations of the NsT-MD results from those of the MOLPAK/WMIN predictions are also given in Table 3. The deviations from the MOLPAK/WMIN result were no greater than 5.6% in cell dimension (solution 1, AK), 1.3° in cell angle, and 8% in density (solution 1, AK, and solution 1, AV).

A more rigorous comparison of the contents of the cells generated through NsT-MD simulations and MOLPAK/WMIN calculations are performed through superposition of the NsT-MD time averaged unit cells onto the MOLPAK/WMIN counterpart using the procedure described by Rice and Sorescu.[28] The factors $\Delta\theta$ and Δx in Table 3 are, respectively, the maximum rigid-body rotational displacement (in °) and translational displacement (in Å) of any of the symmetry-equivalent molecules in the time-averaged unit cell relative to those of the MOLPAK/WMIN counterpart. The time-averaged crystals corresponding to solution 4, CB, and solution 1, AK, had the largest deviations in rigid-body rotational and translational displacements, respectively.

The NsT-MD lattice energies are all higher than the MOLPAK/WMIN results and the densities are consistently lower. These trends can be partially attributed to thermal effects introduced in the MD simulations, whereas the MOLPAK/WMIN calculations represent a 0 K result; thermal expansion should generate lower densities and higher lattice energies. Also, there are differences in interaction energies between the $SAPT(DFT)_{exp\text{-}6}$ and SAPT(DFT) potentials: at the 51 RDX dimer potential energy surface minima listed in the supplementary materials of ref. 10, the root mean square deviation from the *ab initio* computed values was 0.40 and 0.14 kcal mol^{-1}, respectively, whereas the maximum deviations were 1.35 and 0.65 kcal mol^{-1}, respectively. Relative energy rankings of the MOLPAK/WMIN and NsT-MD structures also differ, as is apparent in Fig. 1.

Lattice parameters and density for the experimental crystal are given in Table 3 for comparison with both the *Pbca* low-energy structure from the MOLPAK/WMIN calculations and the corresponding time-averaged structure generated in the NsT-MD simulations. Agreement with experiment for all cell parameters is very good, especially those of the NsT-MD results. The deviations from experiment of the NsT-MD densities and cell edge lengths in the *a*, *b* and *c* directions are −0.8, 0.4, 0.3 and 0.1%, respectively. Deviations from experiment in the MOLPAK/WMIN case are slightly larger (3.0%, −0.7, −0.8 and −1.5%, respectively), partially due to lack of inclusion of thermal effects. Table S2 of the ESI† provides a comparison of time-averaged center-of-mass fractional coordinates and orientational Euler angles with the corresponding experimental values for RDX at 298 K and 1 atm. Agreement with experiment for these parameters is also outstanding, with the largest deviation in molecular orientation occurring for the Euler angle ψ, which differs from experiment by $\sim$2.7°. Also, the largest deviation of the location of the molecular mass center is less than 0.07 Å. This excellent agreement is visualized in Fig. 1 of ref. 9.

Further tests of the SAPT(DFT) potential were performed to assess its ability to predict the temperature and pressure dependences of the RDX crystal. The simulation cells used in

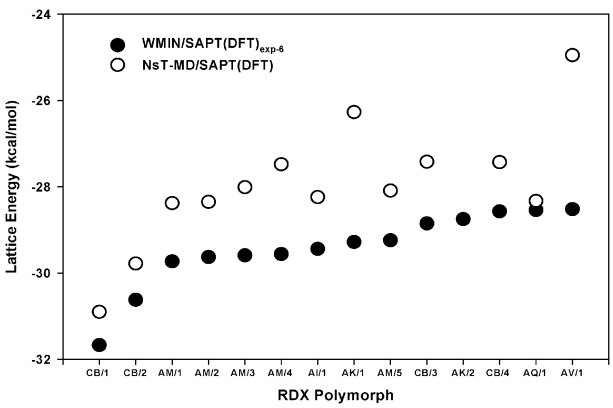

Fig. 1 Lattice energies (kcal mol^{-1}) for the 14 lowest-energy conformers generated by MOLPAK/WMIN. Solid circles denote the results from MOLPAK/WMIN (0 K) calculations using $SAPT(DFT)_{exp\text{-}6}$ and the open circles denote the results from NsT-MD (298 K, 1 atm) simulations using the SAPT(DFT) potential.

Table 4 Temperature-dependent lattice parameters and thermal expansion coefficients (χ)[a]

T/K	a/Å	b/Å	c/Å	α/°	β/°	γ/°	v/Å^3
100	13.1829	11.5526	10.6758	90.00	90.00	90.00	1625.893
200	13.2207	11.5915	10.7133	90.00	90.00	90.00	1641.783
250	13.2385	11.6139	10.7333	90.00	90.00	90.00	1650.244
273.15	13.2487	11.6225	10.7439	90.00	90.00	90.00	1654.368
298	13.2591	11.6338	10.7542	90.01	90.00	89.99	1658.873
325	13.2693	11.6459	10.7670	90.00	90.01	90.00	1663.857
χ^a	28.00 (26.41) [34.8]	33.91 (86.96) [47.5]	34.59 (79.26) [47.2]				95.42 (192.6) [129.6]

[a] Units for linear and volume expansion coefficients are in 10^{-6} K^{-1}. Values in parentheses are derived from experimental measurements given in ref. 29, and values in brackets are theoretical values of Sorescu *et al.*[30]

Table 5 Lattice parameters as functions of pressure

	a/Å			b/Å			c/Å			v/Å^3			α/°	β/°	γ/°
P/GPa	Expt[a]	NsT-MD[b]		Expt[a]	NsT-MD[b]		Expt[a]	NsT-MD[b]		Expt[a]	NsT-MD[b]		NsT-MD[c]		
0.00	13.20	13.2591	(0.4)	11.60	11.6338	(0.3)	10.72	10.7542	(0.3)	1641.446	1658.873	(1.1)	90.01	90.00	89.99
0.73	13.02	13.0701	(0.4)	11.42	11.4568	(0.3)	10.53	10.5561	(0.2)	1564.298	1580.697	(1.0)	90.00	90.00	90.00
1.75	12.89	12.9089	(0.1)	11.22	11.2925	(0.6)	10.27	10.3735	(1.0)	1485.509	1512.182	(1.8)	90.00	90.00	90.00
2.75	12.80	12.8004	(0.0)	11.07	11.1721	(0.9)	10.16	10.2400	(0.8)	1441.190	1464.399	(1.6)	90.00	90.00	90.00
3.36	12.74	12.7484	(0.1)	11.00	11.1106	(1.0)	10.08	10.1701	(0.9)	1413.285	1440.509	(1.9)	90.00	90.00	90.00
3.95	12.67	12.7055	(0.3)	10.93	11.0568	(1.2)	10.03	10.1083	(0.8)	1388.664	1420.041	(2.3)	90.00	90.00	90.00

[a] Ref. 31. [b] Values in parentheses are percent deviations from experimental values. [c] Only predicted cell angles are reported; experimental values are all 90°.

the calculations at various temperatures and pressures were composed of 3 × 3 × 3 crystallographic unit cells and were allowed to equilibrate to the specified thermodynamic condition before properties were calculated and accumulated for averaging. First, a series of NsT-MD calculations were performed over the temperature range 100–325 K. Temperature-dependent crystallographic parameters are given in Table 4. Linear and volume coefficients of thermal expansion (CTE) are extracted from these data and are also given in Table 4 along with experimental[29] and other theoretical values[30] for comparison. We note that the Sorescu *et al.* study[30] reported experimental linear coefficients that are one-third of the reported measured volume CTE value; however, the experimental information indicates that thermal expansion of the lattice is highly anisotropic. Both the work of Sorescu *et al.* and our predictions here indicate anisotropy in the thermal expansion, but to a significantly lesser extent to that observed experimentally. The predicted CTE for the *a* axis is in excellent agreement with the measured value; however, the CTEs for the remaining two axes (and subsequently the volume CTE) are too low by factors of 2–2.5. It is possible that some of the discrepancies could be due to the rigid-molecule approximation imposed in the NsT-MD simulations.

The pressure dependences of the lattice parameters were also calculated for pressures ranging from 0 to 3.95 GPa, and are given in Table 5 along with experimental values. As shown in the table, predicted values in the edge lengths deviate from experiment by no more than 1.2%, and the deviation of the volumes over the pressure range varies from 1–2.3%. A visual comparison with experimental values[31] is given in Fig. 2. The predicted data were fitted to the Murnaghan equation of state

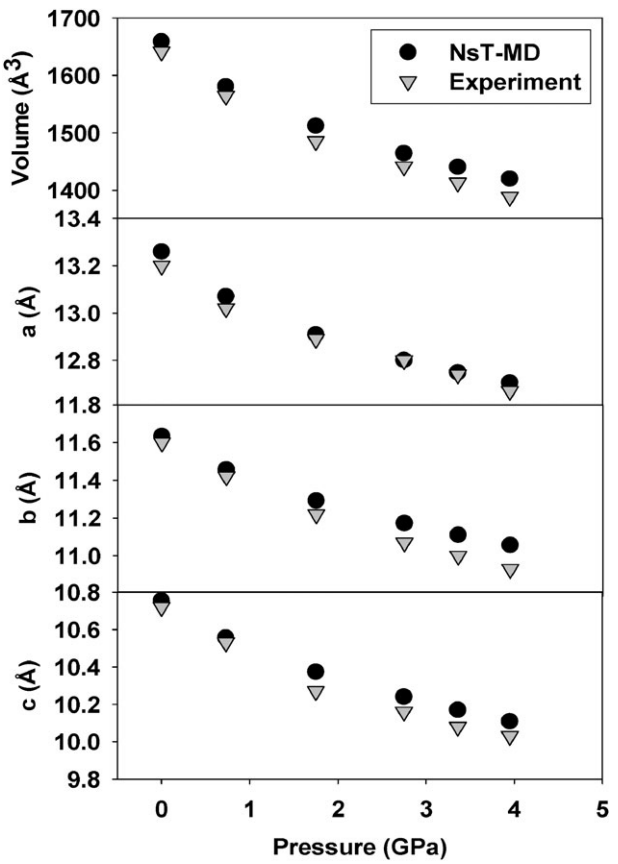

Fig. 2 Variation of predicted and experimental unit cell volume and lattice dimensions with pressure for RDX. Experimental values are taken from ref. 31.

to provide estimates of the bulk modulus B_0 at zero pressure and its pressure derivative B_0'. The predicted values of B_0 and B_0' (12.7 GPa and 8.2, respectively) are in good agreement with reported values derived from experimental measurements (13.0 GPa and 6.6, respectively).[31]

4. Summary

Crystal structure prediction methods employing the MOLPAK/WMIN suite of codes were used to explore various polymorphs of the RDX crystal on the SAPT(DFT)$_{exp\text{-}6}$ potential energy surface. The low-energy crystal produced by these calculations matched the experimental crystal at ambient conditions. This structure, as well as the 13 other lowest-energy crystals generated by these calculations, were used as initial structures in NsT-MD simulations at $T = 298$ K and 1 atm pressure. The NsT-MD simulations used the more elaborate SAPT(DFT) potential energy description.[10] For all but one of the structures, the NsT-MD predictions of crystallographic parameters are in good agreement with the MOLPAK/WMIN predictions, with a maximum 5.6% deviation in cell lengths, 1.3° in cell angles and 8% in densities. Additionally, the space group symmetries are maintained throughout the NsT-MD simulations, except for one case. The NsT-MD results show a slight decrease in density and higher lattice energies, which can be attributed to thermal effects and differences in the potential energy functions. Also, the relative energy rankings differ between the two models; however, the low-energy structures for both sets of calculations correspond to the experimental crystal. The crystallographic parameters and contents of the low-energy crystal produced from the NsT-MD simulations at room conditions matched those of the experimental crystal to within 1% of cell edge lengths and density and 0.01° of cell angles. Further tests of the SAPT(DFT) potential explored its ability to predict the temperature and pressure dependences of the crystallographic parameters of RDX. The results indicated that changes in crystallographic parameters with pressure are similar to experimental values; additionally, the bulk modulus and its pressure derivative are in good agreement with experimentally derived values. Predicted thermal expansion coefficients indicated that expansion of the lattice is only slightly anisotropic, in contrast with experiment. Also, only one of the linear expansion coefficients was in good agreement with experimental values; the remaining two coefficients were substantially smaller than the experimentally derived values. However, it is possible that the thermal expansion behavior might be strongly influenced by intramolecular motion, which was not present in our simulations. The ability of the model to predict the pressure dependence of the lattice parameters is much better, with a maximum deviation of 2.3% in the volume and 1.2% in cell lengths over the entire pressure range that was explored. The success of the SAPT(DFT) potential in describing condensed phase RDX at the ambient state and compressed states provides great incentive to use this approach in developing such analytical potential energy functions for use in atomistic simulations of the condensed phase of other molecular crystals.

Acknowledgements

This research was supported by an ARO DEPSCOR grant, by NSF grant CHE-0555979, by the Polish Science Foundation grant Homing and the Office of Naval Research. Most of the calculations were performed using computer resources allocated by a DoD HPCMP Challenge Project.

References

1 J. Maddox, *Nature*, 1988, **335**, 760.
2 P. Ball, *Nature*, 1996, **381**, 648.
3 G. R. Desiraju, *Nat. Mater.*, 2002, **1**, 77.
4 J. D. Dunitz, *Chem. Commun.*, 2003, 545.
5 X. Wu, M. C. Vargas, S. Nayak, V. L. Lotrich and G. Scoles, *J. Chem. Phys.*, 2001, **115**, 8748.
6 E. F. C. Byrd, G. C. Scuseria and C. F. Chabalowski, *J. Phys. Chem. B*, 2004, **108**, 13100.
7 See, for example: E. F. C. Byrd and B. M. Rice, *J. Phys. Chem. C*, 2007, **111**, 2787, and references therein.
8 S. L. Price, *Int. Rev. Phys. Chem.*, 2008, **27**, 541.
9 R. Podeszwa, B. M. Rice and K. Szalewicz, *Phys. Rev. Lett.*, 2008, **101**, 115503.
10 R. Podeszwa, R. Bukowski, B. M. Rice and K. Szalewicz, *Phys. Chem. Chem. Phys.*, 2007, **9**, 5561.
11 A. J. Misquitta, R. Podeszwa, B. Jeziorski and K. Szalewicz, *J. Chem. Phys.*, 2005, **123**, 214103.
12 A. Hesselmann, G. Jansen and M. J. Schütz, *Chem. Phys.*, 2005, **122**, 014103.
13 R. Podeszwa, R. Bukowski and K. Szalewicz, *J. Chem. Theory Comput.*, 2006, **2**, 400.
14 R. Podeszwa, R. Bukowski and K. Szalewicz, *J. Phys. Chem. A*, 2006, **110**, 10345.
15 R. Podeszwa and K. Szalewicz, *J. Chem. Phys.*, 2007, **126**, 194101.
16 W. B. Schweizer and J. D. Dunitz, *J. Chem. Theory Comput.*, 2006, **2**, 288.
17 A. L. Ringer and C. D. Sherrill, *Chem.–Eur. J.*, 2008, **14**, 2542.
18 A. J. Misquitta, G. W. A. Welch, A. J. Stone and S. L. Price, *Chem. Phys. Lett.*, 2008, **456**, 105.
19 M. A. Neumann, F. J. J. Leusen and J. Kendrick, *Angew. Chem., Int. Ed.*, 2008, **47**, 1.
20 M. A. Neumann and M.-A. Perrin, *J. Phys. B*, 2005, **109**, 15531.
21 See, for example: G. M. Day, W. D. S. Motherwell, H. L. Ammon, S. X. M. Boerrigter, R. G. Della Valle, E. Venuti, A. Dzyabchenko, J. D. Dunitz, B. Schweizer, B. P. van Eijck, P. Erk, J. C. Facelli, V. E. Bazterra, M. B. Ferraro, D. W. M. Hofmann, F. J. J. Leusen, C. Liang, C. C. Pantelides, P. G. Karamertzanis, S. L. Price, T. C. Lewis, H. Nowell, A. Torrisi, H. A. Scheraga, Y. A. Arnautova, M. U. Schmidt and P. Verwer, *Acta Crystallogr., Sect. B*, 2005, **B61**, 511.
22 J. R. Holden, Z. Y. Du and H. L. Ammon, *J. Comput. Chem.*, 1993, **14**, 422.
23 D. L. Cromer, H. L. Ammon and J. R. Holden, *Report LA-11142-MS*, Los Alamos National Laboratory, Los Alamos, NM, 1987.
24 C. S. Choi and E. Prince, *Acta Crystallogr., Sect. B*, 1972, **28**, 2857.
25 H. L. Ammon, MOLPAK software suite and User's Manual, July 2007 version, University of Maryland, College Park, Maryland.
26 W. R. Busing, *Report ORNL-5747*, Oak Ridge National Laboratory, Oak Ridge, TN, 1981.
27 W. Smith, T. R. Forester and I. T. Todorov, *The DL_POLY_2.0 User Manual*, Daresbury Laboratory, United Kingdom.
28 B. M. Rice and D. C. Sorescu, *J. Phys. Chem. B*, 2004, **108**, 17730.
29 H. J. Cady, *J. Chem. Eng. Data*, 1972, **17**, 369.
30 D. C. Sorescu, B. M. Rice and D. L. Thompson, *J. Phys. Chem. B*, 1997, **101**, 798.
31 B. Olinger, B. Roof and H. Cady, *Symposium (Int'l) on High Dynamic Pressures*, C. E. A., Paris, France, 1978, pp. 3–8.

